Free volume in the hard sphere liquid

By SRIKANTH SASTRY[1], THOMAS M. TRUSKETT[1],
PABLO G. DEBENEDETTI[1], SALVATORE TORQUATO[2,3],
and FRANK H. STILLINGER[4,2]

[1] Department of Chemical Engineering, [2] Princeton Materials Institute,
[3] Department of Civil Engineering and Operations Research, Princeton University,
Princeton, NJ 08544, USA
[4] Bell Laboratories, Lucent Technologies, Murray Hill, NJ 07974, USA

A method is developed for the efficient calculation of free volumes and corresponding surface areas in the hard sphere system by extending a previous method for calculating, exactly, cavity volumes in sphere packings. This method is used for the first time to evaluate the free-volume distribution of the hard sphere liquid over a range of densities near the freezing transition. From the distribution of free volumes, the equation of state can be obtained from a purely geometric analysis, which permits the calculation of pressure in Monte Carlo simulations where the dynamic definition cannot be employed. Furthermore, the cavity-volume distributions are obtained indirectly from the free-volume distributions in a density range where direct measurement is inadequate. Direct measurement of the first moment of the cavity-volume distribution makes it possible to calculate the chemical potential in the vicinity of the freezing transition.

1. Introduction

It is well established that the structure of most dense liquids is dominated by repulsive interactions. The simplest model liquid that embodies this feature is the hard sphere fluid, in which impenetrable particles interact solely via hard-core repulsions. The hard sphere system has played a major role in liquid state theory ever since seminal investigations by computer simulation [1–3] suggested strongly that it exhibits a first-order freezing transition. In the late 1950s, comparable strides occurred on the theoretical front with the introduction of the scaled-particle theory of fluids [4], which offered simple and accurate equations of state for systems comprising hard core molecules. These contributions allowed Longuet-Higgins and Widom [5], and later Guggenheim [6], to extend the van der Waals theory by refining the repulsive contribution to the equation of state. In turn, the theories yielded quantitatively accurate predictions for the melting properties of argon.

Following the high-temperature expansions of Zwanzig [7], Barker and Henderson [8, 9] introduced in 1967 their landmark perturbation theory as applied to a simple fluid in which the unperturbed reference system consisted of the positive part of the Lennard-Jones potential, which in turn was related to an essentially equivalent hard sphere system. The remarkable success of the theory of Barker and Henderson demonstrated quantitatively that simple liquids near their triple point are removed by a minor perturbation from a purely repulsive fluid. This result was reaffirmed by the first-order perturbation expansion of Weeks, Chandler and Andersen [10, 11]. These methods inspired researchers [12, 13] to explore in detail the structure of the equilibrated hard sphere fluid. In particular, the perturbation techniques motivated Verlet and Weis [14] to develop a semi-empirical parmeterization of the radial distribution function for the hard sphere liquid, which has become the standard for numerical calculations.

Just as the hard sphere fluid provides a reference for understanding liquid structure, it also represents the simplest system which exhibits a fluid–solid transition and, possibly, a glass transition [15, 16]. The fact that the properties of the hard sphere liquid arise from strictly entropic contributions, that is to say from purely geometric considerations, underlies the continued interest in this system, with recent emphasis directed towards understanding the statistical geometry of dense sphere packings [16–31]. In particular, quantities that describe the *void space* (volume available for insertion of an additional hard sphere), the *free volume* (volume within which a given hard sphere centre can move without requiring alteration of the other sphere positions), and the corresponding surface areas are directly related to thermodynamic quantities.

A computational method has recently been presented by us [32] which permits exact determination of cavity

volumes and surface areas in three-dimensional mono- and polydisperse spherical packings. We utilize this method here to evaluate the chemical potential of the hard sphere liquid over a range of densities near the freezing transition. Furthermore, we extend the above method for the calculation of free volumes and use this information to predict the equation of state of the fluid near the freezing density. We also determine, for the first time exactly, the free-volume distribution in the hard sphere system over a range of densities. The sparsity of void space at high densities renders the cavity-volume distribution statistically inaccessible by the direct approach. However, it will be demonstrated that the cavity-volume distribution can be deduced indirectly from the free-volume distribution, which itself can be determined with a high degree of precision.

In section 2 we present definitions and background information. In section 3 we describe the method for calculating free volumes in sphere packings. The results of our calculations of chemical potentials, pressures, and free- and cavity-volume distributions in the dense hard sphere liquid are presented in section 4. Section 5 contains a summary and concluding remarks.

2. Background

In a system containing N hard spheres, a geometrical *free volume* v_f can be defined [33] as the volume over which the centre of a given sphere can translate, given that the other $N - 1$ spheres are fixed (see figure 1). This should not be confused with the *cavity volume v*, which is the volume of a connected region of space available for the addition of another sphere. By definition, a point is inside of a cavity if it lies outside of the *exclusion spheres* surrounding each particle centre, i.e., if it is separated from each particle centre by at least one hard core diameter σ. At low densities, the void space present in the system is connected, and hence the free volume approaches the void volume. As the density of the system is increased, the void space becomes discon-

nected, corresponding to the percolation of the exclusion spheres. This change in topography of the void space occurs when the exclusion spheres occupy approximately 30% of the space [34], which translates to a reduced density of $\rho_c^* \approx 0.076$ [35], where $\rho^* = N\sigma^3/V$ and V is the system volume. Here, we focus on the statistical geometry of the high-density liquid, i.e., systems well above the percolation threshold.

Speedy and Reiss [36] have demonstrated that the free-volume and cavity-volume distribution functions are related. For completeness, their arguments are reproduced below. In what follows $p(v)\,dv$ is the probability that a cavity has a volume between v and $v + dv$, while $f(v_f)\,dv_f$ is the probability that the free volume of a sphere lies between v_f and $v_f + dv_f$. Analogous probability densities can be defined for the cavity surface $p_s(s)$ and the free surface $f_s(s_f)$.

For a given configuration of spheres, the union volume of the cavities represents the available space V_0. The available surface area S_0 comprises the surface areas of the individual cavities. The average cavity volume and surface area are given by

$$\langle v \rangle = \frac{\langle V_0 \rangle}{N_c} = \int_0^\infty x p(x)\,dx, \qquad \langle s \rangle = \frac{\langle S_0 \rangle}{N_c} = \int_0^\infty y p_s(y)\,dy, \tag{1}$$

where N_c represents the number of cavities in the system, which is averaged over all realizations of the particles. Speedy [37] has shown that the equation of state of an equilibrium hard sphere fluid can be expressed in terms of the statistical geometry of the cavities

$$\frac{\beta P}{\rho} = 1 + \frac{\sigma}{2D} \frac{\langle s \rangle}{\langle v \rangle}, \tag{2}$$

where P is the pressure, ρ is the number density, β is $(kT)^{-1}$, and D is the dimensionality of the system. Stell [38] has made the interesting observation that Boltzmann [39] may have been the first to derive this
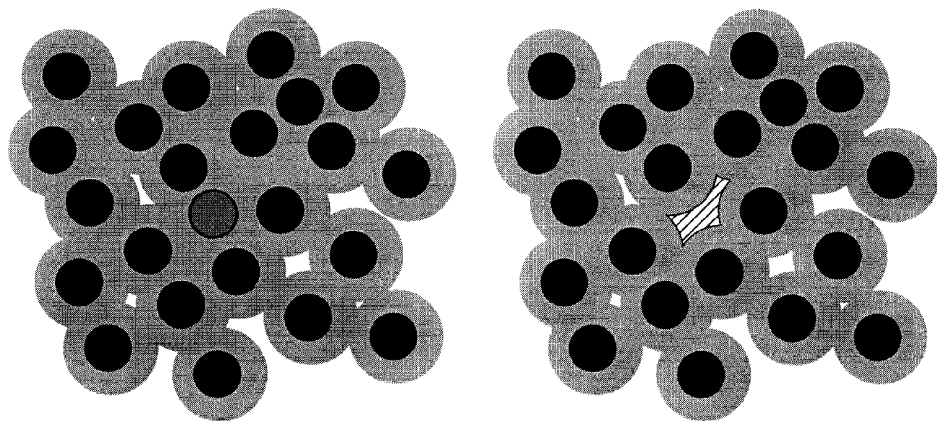

Figure 1. 2D schematic of a configuration of particles with exclusion discs (left). The volume of the cavity that is formed upon removal of the central particle is the free volume v_f of that particle (right). The interface of that cavity is the particle's free surface area s_f.

result. When an additional sphere is added to the system, it enters a cavity of size x which becomes its free volume. Since the sphere additions sample the available space uniformly, a cavity is visited with a frequency that is proportional to its size, i.e.,

$$f(x)\,dx = \frac{x p(x)\,dx}{\int_0^\infty x p(x)\,dx} = \frac{x p(x)\,dx}{\langle v \rangle}. \qquad (3)$$

Strictly speaking, this equation relates the free-volume distribution of a system with $N+1$ spheres to the cavity-volume distribution of the N-sphere system. These two systems become equivalent in the thermodynamic limit.

For any quantity $g(v_f)$ that depends on the free volume, the following relationship holds

$$\langle g(v_f) \rangle = \frac{\int_0^\infty g(x) x p(x)\,dx}{\langle v \rangle} = \frac{\langle v g(v) \rangle}{\langle v \rangle}. \qquad (4)$$

In particular, if we choose $g(v_f) = v_f^n$, then equation (4) yields an equation relating the moments of the free and cavity volume distributions

$$\langle v_f^n \rangle = \frac{\langle v^{n+1} \rangle}{\langle v \rangle}. \qquad (5)$$

From equation (5), it follows that

$$\langle v_f^{-1} \rangle = \langle v \rangle^{-1}, \qquad (6)$$

indicating that the average cavity size is equal to the harmonic mean of the free volume. The surface area that bounds v_f is termed the *free* surface area s_f. Choosing $g(v_f)$ to be the 'free surface'-to-'free volume' ratio reveals the following valuable relationship:

$$\left\langle \frac{s_f}{v_f} \right\rangle = \frac{\langle s \rangle}{\langle v \rangle} = \frac{\langle s_0 \rangle}{\langle V_0 \rangle}, \qquad (7)$$

which was proved originally by Speedy [40] using a slightly different argument. From equations (2) and (7), it is apparent that the pressure can be deduced from free-volume information alone:

$$\frac{\beta P}{\rho} = 1 + \frac{\sigma}{2D} \left\langle \frac{s_f}{v_f} \right\rangle \qquad (8)$$

This equation was suggested 25 years ago by Hoover *et al.* [33] when they considered the dynamics of a *light* particle in a classical system.

The chemical potential of the hard sphere system is directly related also to its statistical geometry:

$$\mu = kT \ln\left(\frac{\lambda^D N}{\langle V_0 \rangle} \right) = kT \ln\left(\frac{\lambda^D N \langle 1/v_f \rangle}{N_c} \right), \qquad (9)$$

where N is the number of particles in the system and λ is the familiar thermal wavelength. The second equality follows from equations (1) and (5) and establishes the connection between the chemical potential and the free-volume distribution. Note that the number of cavities N_c appears in the second relationship, indicating that the chemical potential cannot be determined from free volume information alone. It is conventional to separate the chemical potential μ into an ideal and an excess contribution, i.e.,

$$\mu = \mu^{\mathrm{id}} + \mu^{\mathrm{ex}} = kT \ln\left(\frac{\lambda^D N}{V} \right) + kT \ln\left(\frac{V}{\langle V_0 \rangle} \right). \qquad (10)$$

The former term represents the chemical potential for an ideal gas, while the latter embodies the *reversible work* required to form a cavity of radius σ.

Both analytical and numerical methods have been employed [40–43] to study the cavity volume and free-volume distributions in two dimensions (hard discs). The present work will focus on the exact determination of these quantities for the three-dimensional system.

3. Methodology

The algorithm described below is an extension of the method proposed by Sastry *et al.* [32] to calculate cavity volumes and surface areas in particle packings. For brevity, only a summary of the method is given; the interested reader can find more details in their original paper.

Given a configuration of hard spheres, the first step in the algorithm is the generation of Voronoi and Delaunay tessellations. Both of these constructions divide space into distinct, non-overlapping regions. The Voronoi tessellation divides the system into convex polyhedra which surround each atom. Specifically, a Voronoi polyhedron V_i consists of points closer to atom i than any other atom. There will be several polyhedra V_k which share a face wiith V_i. The atoms corresponding to the neighbouring polyhedra V_k are termed 'geometric neighbours' of atom i. The Delaunay tessellation is obtained by connecting all geometric neighbours, forming a 'primitive graph' of Delaunay simplices (triangles in two dimensions, tetrahedra in three dimensions). A schematic of the dual construction is given in figure 2. A cavity corresponds to a percolation cluster of Voronoi edges that lie entirely within the available space (i.e., outside of the exclusion spheres) [44, 45] Sastry *et al.* [32] have demonstrated that a cavity is enclosed entirely by the Delaunay simplices which are dual to the Voronoi vertices within the cavity.

To calculate the volume and surface area of each cavity, the corresponding Delaunay simplices are sub-
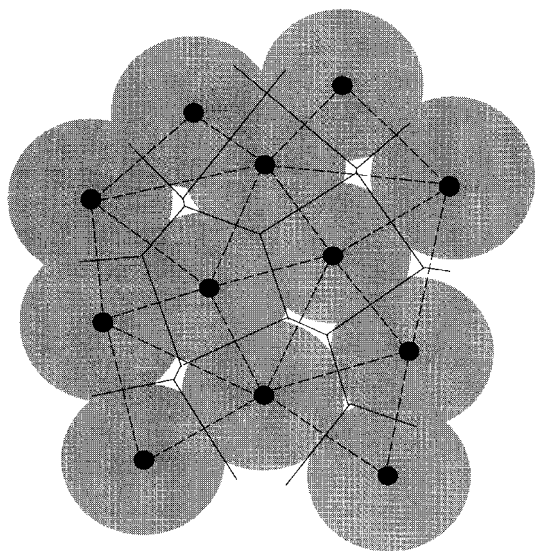
Figure 2.   Typical 2D configuration of exclusion discs is shown with its corresponding Voronoi (solid lines) and Delaunay (dashed lines) tesselations. A set of Voronoi vertices connected by edges that lie entirely within the void region represents a cavity.

Figure 3.   Proof that upon removal of i, only geometric neighbours of i (i.e., k, but not j) must be re-tessellated. See text for discussion.

divided into a set of (generally overlapping) subsimplices. The advantage of this division, which is described in detail elsewhere [32], is that for each subsimplex, only one exclusion sphere must be considered for determining its contribution to the surface area and volume. With an appropriate sign designation, the subsimplex contributions can be added directly to yield the total surface area and volume for each cavity (by design this method avoids the cumbersome calculation of multiple sphere overlaps).

To determine the free volume and the free surface area for a given sphere, the sphere is simply removed from the system. The cavity that contains the centre of the sphere so removed is then analysed using the aforementioned algorithm. Of course, when a sphere is removed from the configuration a local region surrounding the resulting cavity must be *re-tessellated* The efficiency of this routine can be maintained if the region to be re-tessellated is minimal. Fortunately, some properties of the dual tessellation allow for the determination of such a minimal region:

Theorem 1: if an atom is removed from the system, only the Voronoi polyhedra of its geometric neighbours must be re-tessellated.

To see this, consider the removal of atom i from the configuration. By definition, the only Voronoi polyhedra that are affected are those whose atoms are closer to a point in V_i than any other atom. To prove the above theorem, we must demonstrate that at least one geometric neighbour k is closer than any non-neigh-
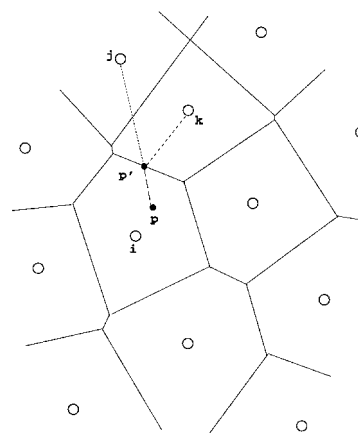
bouring atom j to an arbitrary point p in V_i. Given a point p in V_i, consider the nearest non-neighbouring atom j (see figure 3). If a vector, $\mathbf{r}_{jp}$, is drawn to connect the point of interest to atom j, then it will intersect V_i at some point p'. The point p' will be on the face shared between V_i and V_k, and the definition of V_k requires that $|\mathbf{r}_{jp'}| > |\mathbf{r}_{kp'}|$. Furthermore $|\mathbf{r}_{jp}| = |\mathbf{r}_{jp'}| + |\mathbf{r}_{pp'}|$ and $|\mathbf{r}_{kp}| \leqslant |\mathbf{r}_{kp'}| + |\mathbf{r}_{pp'}|$ (by the triangle inequality). It then follows that $|\mathbf{r}_{jp}| > |\mathbf{r}_{kp}|$, and the theorem is proved.

Theorem 2: Pairs of geometric neighbours of atom i that share a Voronoi face continue to do so after atom i is removed.

Consider atoms k and k' which are geometric neighbours of atom i and share a common face. Any point on the common face is closer to atoms k and k' than any other atom in the system. Clearly the removal of any other atoms (including atom i) will not change this fact, verifying the theorem.

Theorems 1 and 2 indicate that the minimal region in which the tessellation must be reconstructed after the removal of atom i is the superpolyhedron s_i composed of all Delaunay simplices that share atom i as a vertex. This region is illustrated in figure 4. When atom i is removed, the tessellation is reconstructed inside of s_i, and the surface area and volume of the cavity that contained the centre of atom i can be calculated directly.

The above procedure is applied to each atom in the system, for each configuration considered. The procedure described above is very efficient, consuming less than 2 minutes of CPU time per configuration (for 500 hard spheres on an HP 715/100 workstation). In section 4 the results are presented for the equilibrated hard sphere liquid and a modest extension into the metastable region.
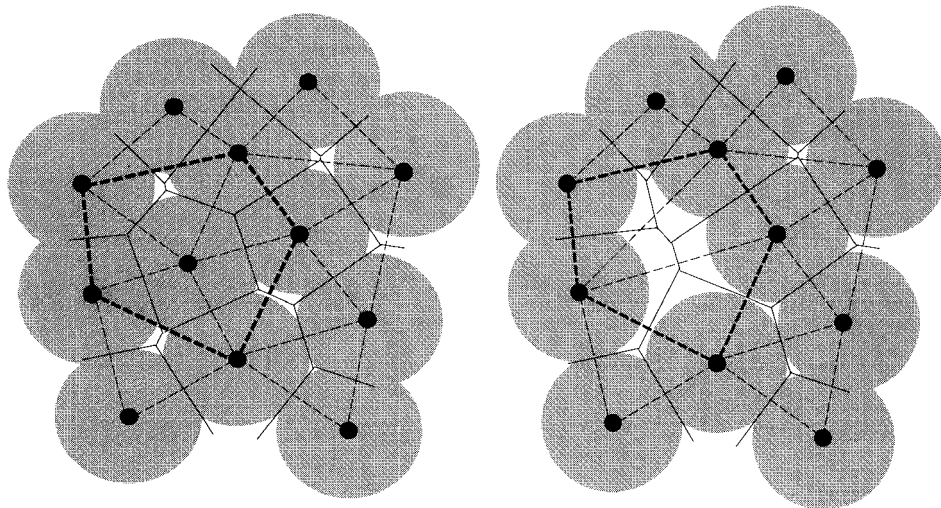
Figure 4. Typical configuration of discs before the central particle is removed (left). After the central particle is removed (right), the tessellation must be reconstructed inside of the superpolyhedron (bold, dashed line). Thus, the volume and surface area of the cavity that once held atom i can be determined.

4. Results for the hard sphere liquid

Systems of $N = 500$ spheres of diameter σ were simulated in a cubic cell of volume V using a standard molecular dynamics (MD) algorithm [31, 46]. The initial configuration was chosen to be a face-centred cubic lattice at a reduced density $\rho^* = 0.80$, where $\rho^* = N\sigma^3/V$. In each case, the lattice was melted by simulating for $5000N$ collisions to obtain the equilibrated fluid. Higher densities were achieved by allowing the diameter of the spheres to increase linearly with time via the prescription of Lubachevsky and Stillinger [46, 47]. This compression protocol will, in general, create a non-equilibrium state at the density of interest. The properties of this state will be an extremely complex function of the system's history. To remove these effects, compressed packings were allowed to relax over a period of $3500N$ sphere collisions, which was sufficient to guarantee reproducible thermodynamic properties.

In order to explore the statistical geometry of the dense liquid, several packing fractions were investigated in the vicinity of the freezing transition ($\rho_f^* \approx 0.943$). In particular, runs were performed at reduced densities $\rho^* = 0.80$, 0.85, 0.90, 0.91, 0.93, 0.943, 0.95, and 0.96. Strictly speaking, any amorphous packing with a density $\rho^* > \rho_f^*$ exists in a state that is metastable with respect to formation of the crystalline phase. However, the entropic barriers to crystallization are large for modest extensions along the metastable branch. Indeed, Speedy [31] has found that metastable hard sphere systems with $\rho^* < 1.03$ will not crystallize even after 10^5 collisions per particle.

As can be seen from equation (8), the equation of state for the hard sphere fluid can be determined from free-volume considerations alone. The exact algorithm presented in section 3 allows for the first direct test of equation (8) by computer simulation. For the calcula-
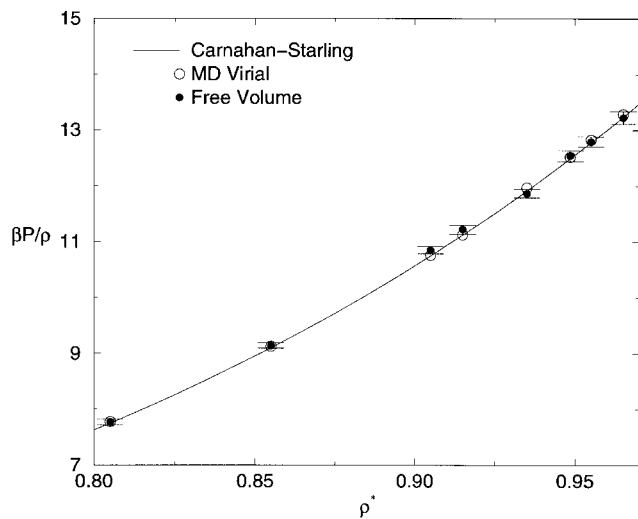

Figure 5. Dimensionless pressure $\beta P/\rho$ of the hard sphere system as calculated from both free-volume information and the molecular dynamics collision rate. The Carnahan–Starling [56] equation is shown also for comparison.

tion of the pressure, 500 configurations (separated by 10^4 collisions each) were stored at each state point. Results for the 500-sphere system are shown in figure 5. Given the relatively small number of configurations considered, the agreement between the pressure calculated from equation (8) and from the virial (collision rate) is remarkable. As a check, the pressure was determined also from the free-volume distributions of configurations generated by a series of Monte Carlo (MC) simulations (see the discussion of the chemical potential results for details on the MC runs). The equations of state produced by the MD and MC routes were statistically indistinguishable. In principle, equation (2) provides yet another geometric route to the equation of
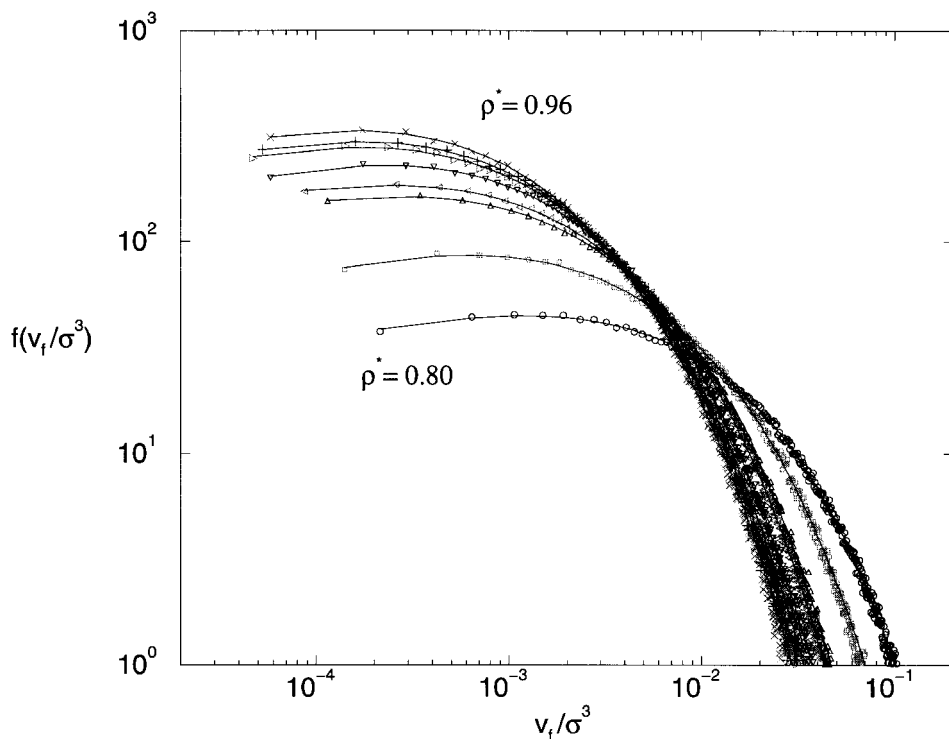
Figure 6. Free-volume distributions for densities $\rho^* = 0.8$, 0.85, 0.9, 0.91, 0.93, 0.943 (freezing density), 0.95, and 0.96. The solid lines represent the fit to equation (12).

state. However, the available space vanishes for many dense configurations of 10^2-10^3 spheres, rendering equation (2) problematic from a sampling viewpoint.

The calculation of the pressure from geometric considerations is crucial for studies of dense systems, in particular for the metastable densities where crystallization occurs readily ($1.03 < \rho^* < 1.11$) [31, 48]. It has been recognized that the statistical mechanical formalism used to describe such states must be modified through the introduction of specific constraints [49–52]. Furthermore, Corti *et al.* [53] have demonstrated that geometrical constraints can be applied to simulate superheated liquids using an MC algorithm. In their investigation, the liquid was prevented from boiling by constraining the size of the largest void in the system. For the metastable hard sphere liquid, the corresponding constraint should prevent the formation of crystallites. Rintoul and Torquato [48] have shown that a bond-orientational order parameter [54] can be invoked to filter out configurations that contain significant crystallization. Due to the need for repeated enforcement of constraints, MC simulations have an obvious advantage over their deterministic counterpart (MD) for simulating metastable phases. However, efficient and accurate methods for calculating the hard sphere equation of state have been lacking in MC simulations, where the dynamic definition cannot be employed. The free-volume algorithm presented here provides one such efficient route to the pressure, requiring only static information.

The distribution of free volumes $f(v_f)$ is shown in figure 6 for densities in the vicinity of the freezing transition. Note that there seems to be a smooth change in the behaviour of the free-volume distributions as the fluid enters the metastable region. It is not known if the free-volume distribution continues to vary in a regular way as the fluid is compressed along the metastable extension of the fluid branch. If a thermodynamic glass transition occurs in the metastable region, it will be a result of structural arrest. Such a profound signature of attenuated particle mobility should be evidenced by a change in form of the free-volume distribution. Studies are underway to probe the statistical geometry of the dense, metastable fluid.

It should be noted that in one dimension the free-volume distribution is known exactly [55], and is given by

$$f(v_f) = \frac{v_f}{\langle v_f \rangle^2} \exp\left(- \frac{v_f}{\langle v_f \rangle} \right). \qquad (11)$$

For dimensions $D > 1$ there are no exact results, although Hoover *et al.* [41] proposed the following form for the free-volume distribution for hard discs (above the percolation threshold):

$$f(v_f) \propto v_f^\alpha \exp\left(- \beta v_f^\gamma \right) \qquad (12)$$

where α is a small and positive constant, and γ is a parameter chosen (in their study) to be unity. We have

found that this simple form describes the exact free-volume distributions in three dimensions accurately, with $\alpha = 0.28$-0.35 and $\gamma = 0.55$-0.45 for the range of densities investigated. It has been pointed out [24] that this expression cannot be correct since it implies, along with equation (3), that the probability of observing a cavity of zero volume diverges, i.e., $p(0) = \infty$. We note that there is no fundamental problem with a probability density diverging, as long as the integrated *probability* is suitably defined for a given interval. More precisely, the probability density must be non-negative and normalize to unity. Hence, the form proposed by Hoover *et al.* [41] is both plausible and accurate for the three-dimensional hard sphere system near its freezing point.

Although the free volume is positive for every particle that is not *rigidly jammed*, the available space is identically zero for many configurations in the dense liquid. Therefore, direct measurement of the *entire* cavity-volume distribution is futile for densities near the freezing transition. Fortunately, equation (3) provides an indirect method for determining the cavity-volume distribution from the free-volume distribution. Results are presented in figures 7 and 8 for the liquid at reduced densities of $\rho^* = 0.8$ and 0.943, respectively. For the system at $\rho^* = 0.8$, the free-volume data provide information about the tail of the distribution where direct sampling fails. As can be seen in figure 8, even less can be determined by direct measurement at the freezing transition. In simulations of reasonable size, the fluctuations which give rise to the tail of the cavity-volume distribution are so rare as to be virtually non-existent.

Although it is difficult to obtain the entire distribution of cavity volumes at high densities, reasonable statistics
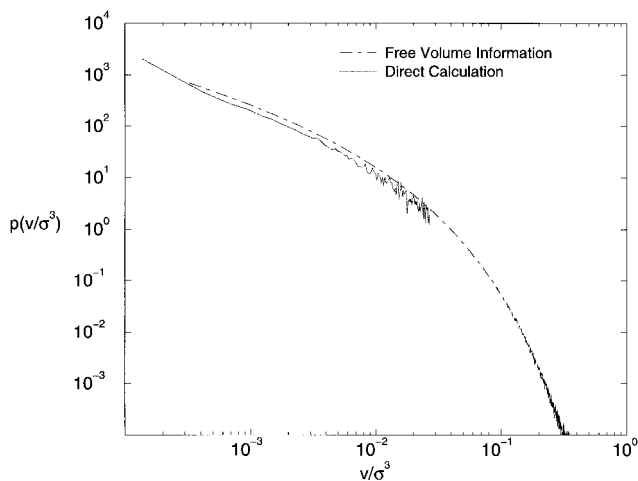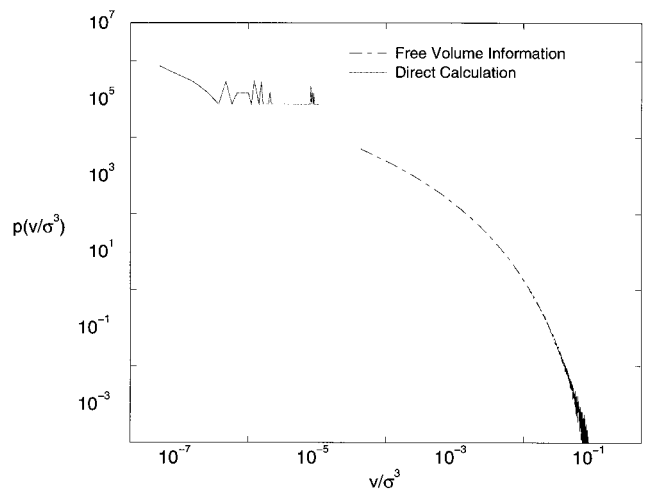

Figure 8. Cavity-size distribution p of the hard sphere fluid at the freezing density $\rho^* = 0.943$ as calculated from free-volume information and direct measurement.

can be obtained for the average cavity size $\langle v \rangle$ and, through equations (1) and (10), the excess chemical potential. This is true, in part, because the large cavities that contribute to the tail of the distribution are indeed rare occurrences. To measure the excess chemical potential directly, 5000 configurations were generated by a standard NVT MC algorithm for the densities $\rho^* = 0.8, 0.85, 0.9, 0.91, 0.93$, and 0.943. For each density, a face-centred cubic lattice was melted for 10^5 MC cycles (attempted moves per particle). The configurations were saved in intervals of 200 cycles during a 10^6 cycle production run.

The available volume of each configuration was measured via the method of Sastry *et al.* [32], and the excess chemical potential μ^{ex} was determined using equation (10). The results are presented in figure 9 along with the excess chemical potentials consistent with the accurate hard sphere equations of state developed by Carnahan and Starling [56] and Sanchez [57]. For comparison, the precise calculations of Attard [58] and Labik and Smith [59] are shown also. The standard deviation was estimated by blocking the configurations into 20 subsets. As can be seen, good agreement is obtained for all densities, including the freezing transition.

5. Conclusion

A methodology for determining exactly the free volume and free surface area of a given particle in a configuration of hard spheres is presented. Using previously derived identities [36, 39, 40] that relate the statistics of the free-volume distribution to the hard sphere equation of state, the pressure was determined in the vicinity of the freezing transition. The efficiency of this algorithm allows for the pressure to be determined pre-

Figure 7. Cavity-size distribution p of the hard sphere fluid at density $\rho^* = 0.8$ as calculated from free-volume information and direct measurement.
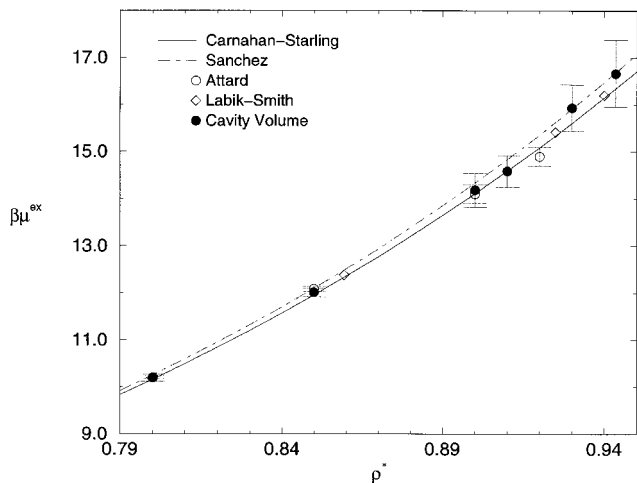
Figure 9.   Excess chemical potential μ^{ex} is shown as calculated from the cavity-volume statistics. The excess chemical potential consistent with the Carnahan–Starling [56] and Sanchez [57] equations of state along with accurate data obtained by the methods of Attard [58] and Labik-Smith [59] are shown for comparison.

cisely in an MC simulation, where the collision rate is inaccessible.

Free volume distributions for the dense, hard sphere fluid are characterized for the first time. The distributions provide an indirect route to information about the statistics of *cavity* volumes. This is significant because the infrequent appearance of void space at high densities prevents the direct measurement of such quantities. Characterization of both cavity- and free-volume distributions should prove to be interesting for metastable sphere systems, where the statistical geometry is poorly understood.

It is shown that the first moment of the cavity-volume distributions, i.e., the average cavity size, can be obtained by direct measurement. This quantity was calculated for the hard sphere liquid in the vicinity of the freezing transition. From this information the excess chemical potential was determined and was found to be in good agreement with previously tabulated results.

References

[1] ALDER, B. J., and WAINWRIGHT, T. E., 1957, *J. chem. Phys.*, **27**, 1208.
[2] ALDER, B. J., and WAINWRIGHT, T. E., 1962, *Phys. Rev.*, **127**, 359.
[3] HOOVER, W. G., and REE, F. H., 1968, *J. chem. Phys.*, **49**, 3609.
[4] REISS, H., FRISCH, H. L., and LEBOWITZ, J. L., 1959, *J. chem. Phys.*, **31**, 369.
[5] LONGUET-HIGGINS, H. C., and WIDOM, B., 1964, *Molec. Phys.*, **8**, 549.
[6] GUGGENHEIM, E. A., 1965, *Molec. Phys.*, **9**, 43.
[7] ZWANZIG, R. W., 1954, *J. chem. Phys.*, **22**, 1420.
[8] BARKER, J. A., and HENDERSON, D., 1967, *J. chem. Phys.*, **47**, 4714.
[9] BARKER, J. A., and HENDERSON, D., 1976, *Rev. mod. Phys.*, **48**, 587.
[10] CHANDLER, D., WEEKS, J. D., and ANDERSEN, H. C., 1983, *Science*, **220**, 787.
[11] CHANDLER, D., WEEKS, J. D., and ANDERSEN, H. C., 1976, *Adv. chem. Phys.*, **34**, 105.
[12] BARKER, J. A., and HENDERSON, D., 1971, *Molec. Phys.*, **21**, 187.
[13] STILLINGER, F. H., 1971, *J. comput. Phys.*, **7**, 367.
[14] VERLET, L., and WEIS, J.-J., 1972, *Phys. Rev. A*, **5**, 939.
[15] WOODCOCK, L., 1981, *Ann. N.Y. Acad. Sci.*, **371**, 274.
[16] SPEEDY, R. J., 1993, *Molec. Phys.*, **80**, 1105.
[17] HIWATARI, Y., SAITO, T., and UEDA, A., 1984, *J. chem. Phys.*, **81**, 6044.
[18] REISS, H., and HAMMERICH, A. D., 1986, *J. phys. Chem.*, **90**, 6252.
[19] TOBOCHNIK, J., and CHAPIN, P., 1988, *J. chem. Phys.*, **88**, 5824.
[20] ZHOU, Y., and STELL, G., 1988, *J. statist. Phys.*, **52**, 1389.
[21] TORQUATO, S., LU, B., and RUBINSTEIN, J., 1990, *Phys. Rev. A*, **41**, 2059.
[22] GONZALEZ, D. J., and GONZALEZ, L. E., 1991, *Molec. Phys.*, **74**, 613.
[23] NEZBEDA, I., and SMITH, W. R., 1992, *Molec. Phys.*, **75**, 789.
[24] BOWLES, R. K., and SPEEDY, R. J., 1994, *Molec. Phys.*, **83**, 113.
[25] YEO, J., 1995, *Phys. Rev. E*, **52**, 853.
[26] TORQUATO, S., 1995, *Phys. Rev. E*, **51**, 3170.
[27] RINTOUL, M. D., and TORQUATO, S., 1996, *Phys. Rev. Lett.*, **77**, 4198.
[28] YUSTE, S. B., DE HARO, M. L., and SANTOS, A., 1996, *Phys. Rev. E*, **53**, 4820.
[29] DASGUPTA, C., and VALLS, O. T., 1996, *Phys. Rev. E*, **53**, 2603.
[30] REISS, H., ELLERBY, H. M., and MANZANARES, J. A., 1996, *J. phys. chem.*, **100**, 5970.
[31] SPEEDY, R. J., 1997, *J. Phys.: Condens. Matter*, **9**, 8591.
[32] SASTRY, S., CORTI, D. S., DEBENEDETTI, P. G., and STILLINGER, F. H., 1997, *Phys. Rev. E*, **56**, 5524.
[33] HOOVER, W. G., ASHURST, W. T., and GROVER, R., 1972, *J. chem. Phys.*, **57**, 1259.
[34] SEVICK, E. M., MONSON, P. A., and OTTINO, J. M., 1988, *J. chem. Phys.*, **88**, 1198.

[35] LEE, S. B., and TORQUATO, S., 1988, *J. chem. Phys.*, **89,** 3258.

[36] SPEEDY, R. J., and REISS, H., 1991, *Molec. Phys.*, **72,** 1015.

[37] SPEEDY, R. J., 1980, *J. chem. Soc. Faraday Trans* II, **76,** 693.

[38] STELL, G., 1966, *Lecture Notes* (New York: Polytechnic Institute of Brooklyn).

[39] BOLTZMANN, L., 1964, *Lectures on Gas Theory*, translated by S. Brush (University of California Press).

[40] SPEEDY, R. J., 1981, *J. chem. Soc. Faraday Trans II*, **77,** 329.

[41] HOOVER, W. G., HOOVER, N. E., and HANSON, K., 1979, *J. chem. Phys.*, **70,** 1837.

[42] STURGEON, K. S., and STILLINGER, F. H., 1992, *J. chem. Phys.*, **96,** 4651.

[43] RINTOUL, M. D., and TORQUATO, S., 1995, *Phys. Rev.* E, **52,** 2635.

[44] KERSTEIN, A. R., 1983, *J. Phys.* A, **16,** 3071.

[45] MEDVEDEV, N. N., 1994, *Dokl. Akad. Nauk*, **337,** 767 (English translation: 1994, *Dokl. phys. Chem.*, **337,** 157).

[46] LUBACHEVSKY, B. D., and STILLINGER, F. H., 1990, *J. statist. Phys.*, **60,** 561.

[47] LUBACHEVSKY, B. D., and STILLINGER, F. H., 1991, *J. statist. Phys.*, **64,** 501.

[48] RINTOUL, M. D., and TORQUATO, S., 1996, *J. chem. Phys.*, **105,** 9258.

[49] SCHAAF, P., and REISS, H., 1990, *J. chem. Phys.*, **92,** 1258.

[50] STILLINGER, F. H., 1995, *Comput. Mater. Sci.*, **4,** 383.

[51] STILLINGER, F. H., 1995, *Science*, **267,** 1935.

[52] DEBENEDETTI, P. G., 1996, *Metastable Liquids* (Princeton, NJ: Princeton University Press).

[53] CORTI, D. S., DEBENEDETTI, P. G., SASTRY, S., and STILLINGER, F. H., 1997, *Phys. Rev. E*, **55,** 5522.

[54] STEINHARDT, P. J., NELSON, D. R., and RONCHETTI, M., 1983, *Phys. Rev.* B, **28,** 784.

[55] SPEEDY, R. J., and REISS, H., 1991, *Molec. Phys.*, **72,** 999.

[56] CARNAHAN, N. F., and STARLING, K. E., 1969, *J. chem. Phys.*, **51,** 635.

[57] SANCHEZ, I. C., 1994, *J. chem. Phys.*, **101,** 7003.

[58] ATTARD, P., 1993, *J. chem. Phys.*, **98,** 2225.

[59] LABIK, S., and SMITH, W. R., 1994, *Molec. Simulation*, **12,** 23.